Nitrogen Fixation at Paleo-Mars in Icy Climates

Danica Adams[1,2,*], Armin Kleinböhl[3], Franklin P Mills[4,5], Run-Lie Shia[2], King-Fai Li[6], Robin Wordsworth[1], Yuk Yung[2,3]

[1]Harvard University, Department of Earth and Planetary Sciences
[2]Caltech, Division of Geological and Planetary Sciences
[3]Jet Propulsion Laboratory, California Institute of Technology
[4]Australian National University, Fenner School of Environment & Society
[5]Space Science Institute
[6]University of California Riverside, Department of Environmental Science

Abstract

Recent findings by the Mars Science Laboratory (MSL) have confirmed the presence of nitrates near Gale Crater on Mars. In this work, we consider the formation and deposition of HNOx species in cold early Mars climates. We find that solar energetic particles could facilitate nitrogen fixation by photochemically generating pernitric and nitric acid, which then deposit onto icy particles that settle onto Mars' surface. This study demonstrates that such deposition would be more efficient under higher atmospheric pressures, consistent with Mars' ancient atmosphere, and could account for the nitrate levels detected by the MSL. We find a more rapid deposition rate for pernitric acid over nitric acid (in agreement with Smith et al., 2014), and a significant enhancement of deposition rates through consideration of deposition onto icy particles. This distinction could be crucial for interpreting the MSL data.

Plain Language Summary

The MSL rover has detected NO from in surface soils, which is thought to come from nitrate in the soil. In this work, we make new estimates for deposition of pernitric acid in icy climates, and we discuss implications for interpreting the MSL measurements.

1. Introduction

Evolved gas analysis measurements of Mars' soils made by the Sample Analysis at Mars (SAM) instrument on board the Mars Science Laboratory (MSL) recently discovered 70-260 and 330-1100 ppm of nitrate in the Klein and Cumberland Noachian-aged mudstone deposits, respectively, at Yellowknife Bay (Stern et al., 2015). Subsequent measurements of 0.002 to 0.05 wt% of nitrate in sediments near Gale Crater were also reported (Sutter et al., 2017). The presence of nitrate suggests a nitrogen cycle during Mars' history. This would be relevant to astrobiology, as nitrogen fixation is required for nitrogen to be useful to terrestrial life (e.g., Holm & Neubeck, 2009; Mancinelli & McKay, 1988). However, the precise mechanism of the nitrogen cycle on early Mars remains debated.

Adams et al. (2021) recently described how these nitrates could have been formed by lightning-induced nitrogen fixation in a warm and wet climate. The assumed warm climate was motivated by significant geochemical and geomorphological evidence that suggests warm wet climate episodes of 10^5-10^7 years duration (e.g., Carr et al., 2003; Clifford et al., 2001; Barnhart et al., 2009; Hoke et al., 2011; Olsen et al., 2007). However, the globally averaged surface deposits of nitrate predicted by Adams et al. (2021) are consistent only with the lower limits of the MSL measurements, and the climate would have likely only been warm and wet for a brief

window of Mars' history (e.g., Wordsworth et al., 2016). Since cold, icy climates likely persisted for longer during Mars' total history, it remains interesting to examine whether nitrates could have formed during the cool periods too.

Mancinelli (1996) predicted the formation of nitrates at early Mars would arise via the following chemical pathways: First, photodissociation of N_2 and ion-neutral reactions are known to form odd nitrogen radicals in the thermosphere, and upon transporting downwards, these species may then be oxidized to form nitric acid (e.g., Krasnopolsky, 1993; Yung et al., 1977). Smith et al. (2014) also considered formation and dry deposition of nitric and pernitric acid in 7 and 35 mbar Amazonian atmospheres. They found dry deposition of the latter exceeded the former by two orders of magnitude and N accumulation during the Amazonian of 0.4-0.2 wt% if mixed uniformly to a depth of 1.5-2.6 m. In this work, we seek to improve estimates by considering: five climate scenarios with surface pressures ranging from 7 mbar - 1 bar (representative of Mars' climate change through time from Noachian to Amazonian); adding energy deposition from solar energetic particles; and adding adsorption of HNOx species onto atmospheric ice particles which settle onto Mars' surface.

2. Methods

We adapt KINETICS, the Caltech/JPL chemical transport model (e.g., Allen et al., 1981), to a 1D and diurnally-averaged present-day Mars environment as in Nair et al. (1994). KINETICS has been applied to and validated against data for many other worlds including Jupiter (e.g., Moses et al., 2005), Titan (e.g., Li et al., 2014), and Pluto (see, e.g., Wong et al., 2015), and a similar approach was considered for nitrogen fixation in warmer climates for the early Earth in Wong et. al. (2017) and for early Mars in Adams et al. (2021).

The model solves the 1D continuity equation by computing the chemical production and loss rates at each layer, as well as the diffusive flux between each layer:

$$\frac{dn_i}{dt} = P_i - L_i - \frac{\partial \phi_i}{\partial z}, \quad (1)$$

where n_i is the number density of species i, P_i the chemical production rate, L_i the chemical loss rate, and ϕ_i the vertical flux, all considered at time t and altitude z. The vertical flux is given by

$$\phi_i = -D_i\left(\frac{\partial n_i}{\partial z} + \frac{n_i}{H_i} + \frac{1-\alpha_i}{T}\frac{\partial T}{\partial z}n\right) - K_{zz}\left(\frac{\partial n_i}{\partial z} + \frac{n_i}{H_a} + \frac{1}{T}\frac{\partial T}{\partial z}n\right), \quad (2)$$

where D_i is the species' molecular diffusion coefficient, H_i the species' scale height, α_i the thermal diffusion parameter, H_a the atmospheric scale height, T the temperature, and K_{zz} the vertical eddy diffusion coefficient, (Yung & DeMore, 1999). The flux consists of molecular diffusion (which is derived from the molecular theory of ideal gases) and eddy transport. We calculate the eddy diffusion coefficient profile according to the formulation in Ackerman and Marley (2001). The two terms largely differ according to the scale height: eddy diffusion follows the bulk atmospheric scale height (H_a) which leads to a well-mixed atmosphere, but molecular diffusion drives each species to follow its own scale height (H_i) which drives the system toward diffusive equilibrium in the case of an isotherm.

We investigate icy nitrate formation in five cold climates: 7 mbar, 50 mbar, 200 mbar, 500 mbar, and 1 bar, and we consider the chemistry of the following species linked by 152 reactions on an altitude grid with 1-2 km spacing up to 118 km: O, O(1D), O_2, O_3, H_2O, H, H_2, OH, HO_2, H_2O_2, N, N(2D), NO, NO_2, NO_3, N_2O, N_2O_5, HNO_2, HNO_3, HO_2NO_2, CO, O^+, O_2^+,

CO_2^+, CO_2H^+, and electrons. The full reaction list and the column rates are provided in Table S1. We fix the mixing ratios of N_2 and CO_2 to 2.7 and 97.3% according to the annual mean of present day measurements, ignoring the presence of Ar (Trainer et al., 2019) and to 10 and 90% in the thicker atmospheric cases motivated by previous works that suggest larger N_2 abundances in the past (e.g., Hu & Thomas, 2022). We fix the concentration of H_2O to the saturation vapor pressure in the lower atmosphere and assume it becomes cold trapped to a steady mixing ratio in the stratosphere. We adopt the temperature-pressure profiles computed by Adams et al*., in review*, which used a 1D radiative-convective model to compute the TP profiles expected by the steady state chemistry in each case. We consider their CO_2 dominated atmospheres with low H_2 content, and these TP profiles look similar to profiles in previous radiative-convective simulations (e.g., Kasting, 1991; Wordsworth et al., 2017). Unless otherwise stated, we set the flux at the upper and lower boundaries for each species to be zero. At the lower boundary, we fix the concentration of water vapor to the concentration equivalent to the saturation vapor pressure and the concentration of all ion species to zero. We consider a deposition velocity of nitrous, nitric, and pernitric acid of 0.02 cm s^{-1} (Krasnopolsky 1993; Smith 2014), and a small deposition velocity for O_2, O_3, and CO of 10^{-6} $cm^{-2}s^{-1}$. We consider a flux of N and $N^{(2D)}$ into the atmosphere at the upper boundary to represent deposition of solar energetic particles, and which we estimate from the Geant4 simulation results in Adams et al. (2021). In the 7-mbar case we set the mixing ratios of O_2, H_2, and CO at the lower boundary according to present day measurements. At the upper boundary, we fix the escape flux of O to $1.2x10^8$ molecules cm^{-2} s^{-1} (Nair et al., 1994), which is in agreement with present-day observations (e.g., Jakosky et al., 2018; references therein), and we fix the escape velocity of H and H_2 to $3.08x10^3$ and $3.39x10^1$ cm s^{-1}, respectively, according to diffusion-limited escape theory (e.g., Hunten et al., 1972). We consider that the solar spectrum will have changed over time, assigning an earlier flux (3.8 Ga) for the 500 and 1000 -mbar cases, intermediate-age (2.7 Ga) for the 50 and 200 mbar cases, and a present-day flux for the 7-mbar case. We parametrize these changes according to Claire et al. (2012). We fix the ice particle distribution, and we assume all HNOx deposited onto ice is eventually lost.

Water ice amounts are based on profile retrievals of water ice extinction from measurements by the Mars Climate Sounder (MCS) (Kleinböhl et al. 2009, 2017). We average MCS observations for Mars years 29-33 for the 5 Ls periods 0-5, 45-50, 90-95, 135-140, and 175-180 and compute number densities and cross-sections of ice particles based on the particle size distribution from Kleinböhl et al. (2011) with an effective particle radius of 1.41 microns. We prescribe a rate coefficient for loss of a species through heterogeneous reactions with ice aerosols as:

$$J' = \frac{1}{4}\,\gamma\,\nu\,\sigma\,N_{ice} \quad (3)$$

where γ describes the sticking coefficient, ν describes the thermal velocity of the gas, σ describes the average cross section (area) of the ice particle, and N_{ice} describes the number density of the ice particles (e.g., Yung & DeMore 1982). We consider a γ of 0.01 according to Michelangeli et al. (1989). The computed time-averaged J' profile is plotted in black in Figure

S1, and the temporal variations are overlaid behind in various colors. The earlier atmospheres would have likely hosted greater ice concentrations due to the higher pressures; due to the uncertainty, we scale the present-day ice concentrations by a factor *f* which we vary over 1x, 3x, and 10x for all climate scenarios considered.

3. Results: Photochemical Production of Nitric and Nitrous Acid

The destruction of N_2 is driven by solar energetic particles (SEPs) in the upper atmosphere, and the products are oxidized to produce NO. NO may directly produce HNO_2 through reacting with OH, or it may produce the other NOx species through reactions with O and HO_2. Some NO may also react with N to form N_2O, and which often cycles the fixed-N back to N_2 through photolysis and reactions with $O(^1D)$. N_2O reacting with $O(^1D)$ may also form 2 NO. NO_2 contributes to formation of both nitrous acid (HNO_2) and pernitric acid (HO_2NO_2) through reactions with HO_2, and in a self-terminating reaction the NOx species NO_2 and NO_3 form N_2O_5. While NO_3 and N_2O_5 are both generally susceptible to destruction by photolysis, this N_2O_5 may also react with water vapor or heterogeneously with water ice to produce nitric acid (HNO_3). The HNO_x species may then be absorbed onto ice particles and deposited to the surface. These chemical pathways are summarized in Figure 1.

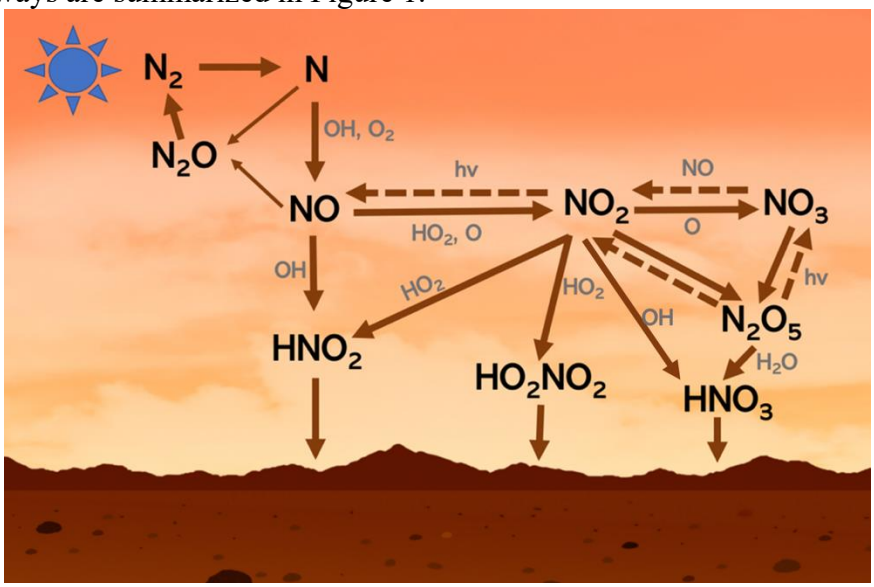

Figure 1. Cartoon of the relevant odd-nitrogen chemistry in Mars' atmosphere. N_2 dissociation by SEPs causes NO formation, oxidation of which leads to HNOx production and deposition.

The steady state mixing ratios which result from this chemistry are shown in Figure 2. The energy deposited and thereby the rate of N_2 destruction is the same in all climate scenarios, causing N and NO mixing ratios to become smaller in the denser atmospheres. In the thicker atmospheres, collisions are more frequent causing the availability of N to become limited to higher altitudes only. For similar reasons, the NO profile (sourced by N) tends to curve back to lower values near the surface in the atmospheres of higher surface pressure. The availability of NO decreases slower than that of N due to both a greater availability of HOx in the thicker atmospheric cases, since its production rate scales with the concentrations of both N and the oxidant, as well as the additional source of NO from N_2O photolysis. For similar reasons, the mixing ratios of HNOx are relatively more consistent across the different atmospheric densities.

For example, in the case of the lowest ice concentration (solid pink lines), the near-surface HO_2NO_2 is near ~10^{-12} (within a factor of ~3) for all atmospheric pressures. However, in the cases with more ice in the 200 mbar atmosphere, the limited availability of lower atmosphere N and NO causes much smaller near-surface mixing ratios of HNOx species. The ice content not only removes HNOx faster but also H_2O_2 and HO_2, which influences the redox state of the atmosphere and slows the reactions which oxidize N and NO. Additionally, in thinner atmospheric cases, the lower density and constant destruction rate of N_2 makes NO more likely to collide and react with N, which forms N_2O and ultimately recycles the NOy species back to N_2. Therefore, in thicker atmospheric cases, a greater fraction of the produced NO will go on to form nitrous and nitric acid. The formation of nitric acid requires reactions with water vapor, and the thicker atmospheric cases foster greater saturation vapor pressures of water. (The water vapor also extends to higher altitudes in the cases of higher pressure, but this is less significant since the N- and NOx- availability also become more limited to higher altitudes in these cases due to more frequent collisions.) Therefore, the steady state mixing ratios of nitric acid are greater in the 500-mbar case than the 50- and 200-mbar cases.

The cases with greater ice abundances result in faster loss of HNOx and N_2O_5, partially due to the adsorption onto the particles and heterogeneous reactions, respectively. The larger ice abundance also causes faster removal of H_2O_2, causing a decrease in OH and atmospheric oxidants. This causes a small increase in N and contributes to slower production of NO and HNOx species, which are largely produced through reactions with HOx.

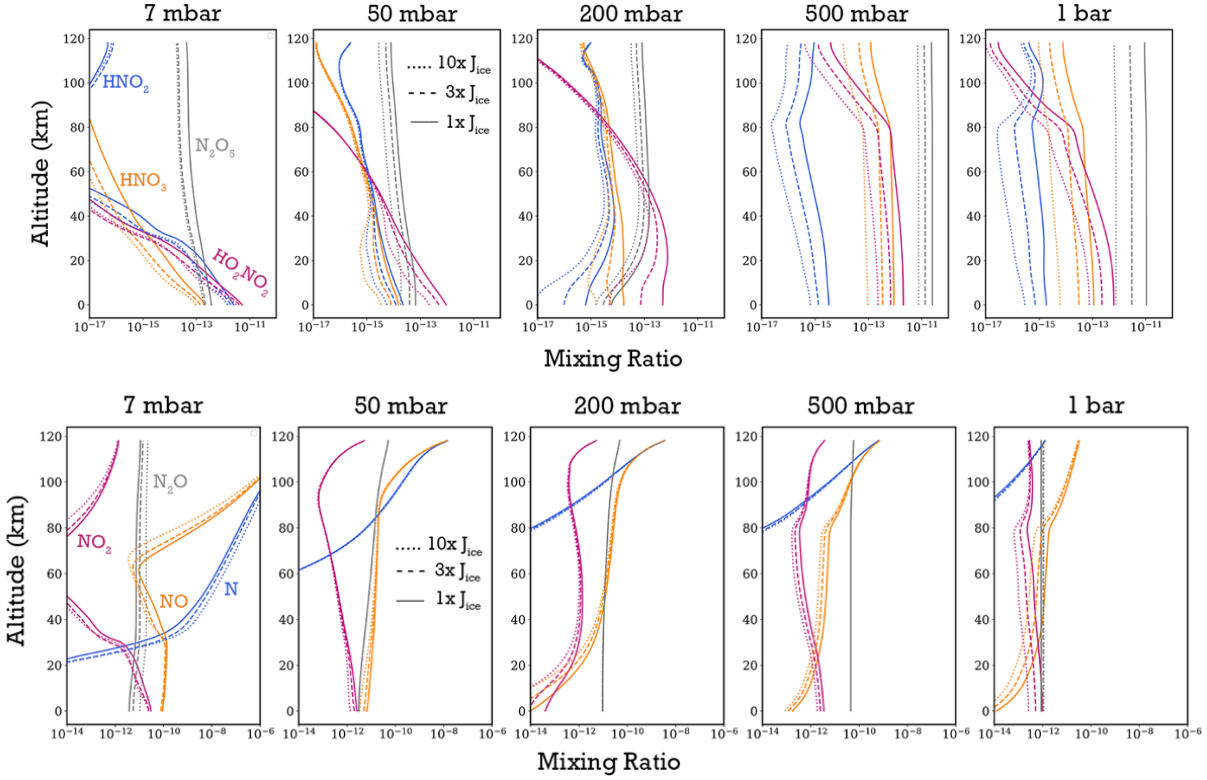

Figure 2. Mixing ratios of nitrous acid (blue), nitric acid (orange), pernitric acid (magenta), and N_2O_5 (grey) are shown in the upper panels. Mixing ratios of N (blue), NO (orange), NO_2 (magenta), and N_2O (grey) are shown in the lower panels. Five climate scenarios are considered from left to right: 7 mbar, 50 mbar, 200 mbar, 500 mbar, and 1 bar. In each panel, the ice

concentration is varied from 1x (solid), 3x (dashed), and 10x (dotted linestyle) the temporal average from MCS data as described in Figure S1.

4. Results: Deposition Rate of HNOx on Ice Particles

We find that deposition of HO_2NO_2 generally dominates the flux of HNO_x species to Mars' surface in icy climates, as summarized in Figure 3. This differs from terrestrial chemistry, where nitric acid deposition is faster than that of pernitric acid because of rapid thermal decomposition in the lower troposphere; however, this rate has a strong temperature dependence and is orders of magnitude slower from tens of degrees of cooling (Graham et al., 1978; Gierczak et al., 2005). The rate of thermal decomposition of HO_2NO_2 in the cool 1-bar early Mars atmosphere is slower than photolysis at the surface by more than 2 orders of magnitude at 200 K and by ~4 orders of magnitude at 180 K. This HO_2NO_2 is formed fastest in the thicker atmosphere cases due to a pressure dependence of the rate for its main production pathway: $HO_2 + NO_2 + M \rightarrow HO_2NO_2 + M$. On the other hand, the formation of nitric acid at early Mars occurs through several reactions, all of which are slower than pernitric acid production: In the thicker atmospheres, N_2O_5 may react with water to form nitric acid, but this is primarily limited to the lowest ~20 km, where water vapor concentrations are largest. In the thin atmospheres, both water vapor and N_2O_5 abundances are low and instead, production of HNO_3 near the surface requires that NO_3 become oxidized by HO_2; however, the NO_3 concentrations are smaller than NO_2 by several orders of magnitudes (thereby again favoring pernitric acid over nitric acid formation). In all cases, nitric acid production in the upper atmosphere (which is relatively dry) is limited to oxidation of NO_2 by OH, but like other HNOx species, the near-surface production (by the previously mentioned reactions) is faster.

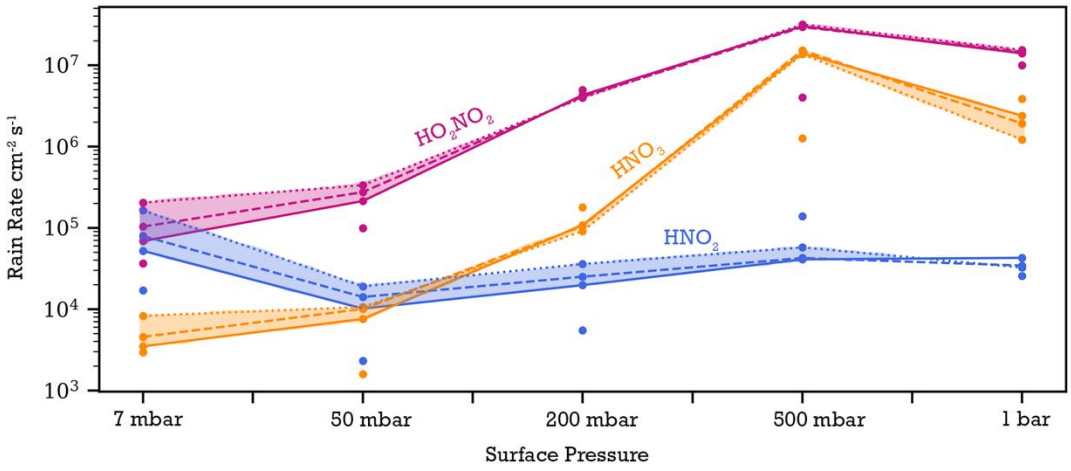

Figure 3. Rate of deposition of HNOx species on ice particles to the Mars surface (cm^{-2} s^{-1}) in five climate scenarios: 7 mbar, 50 mbar, 200 mbar, 500 mbar, and 1 bar. Cases with no ice particles are shown in the unconnected dots. Cases with ice particles are shown in three linestyles for each value of *f*: 1x in solid, 3x in dashed, 10x in dots.

The deposition rates of both pernitric and nitric acid to the surface largely increase as the atmospheric pressure increases. Loss of all HNO_x species is primarily by photolysis, which is much faster than loss to ice particles; however, photolysis rates are relatively consistent between the 50-, 200-, and 500-mbar cases (see Figure 4). Therefore, this trend in deposition rates must

be driven by the production rates. HO_2NO_2 is primarily formed when HO_2 attacks NO_2, and this reaction occurs ~10x faster in the 500 mbar case than in the 50 mbar case (see Figure 4) primarily due to a pressure dependence of the 3-body reaction: $HO_2 + NO_2 + M$. The concentration of NO_2 also influences this rate. NO_2 is larger in the thicker atmospheres (500 mbar and 1 bar) due to greater amounts of O_3 available to oxidize NO to NO_2 compared to the thinner cases (7 and 50 mbar). However, the 200-mbar case sees a depletion in NO_2 due to a limited availability of HOx in the upper atmosphere, which limits conversion from N to NO. This may be due to a larger CO abundance, where the greater CO_2 photolysis rate depletes the upper atmosphere of oxidants in order to convert CO back to CO_2. The production of nitric acid is faster in the thicker atmospheres largely due to the reaction $N_2O_5 + H_2O$ becoming the dominant pathway (see Figure 4). This is attributed to a greater availability of surface liquid water (directly caused by the greater pressures) and of N_2O_5. The near-surface N_2O_5 concentration increases with surface pressure with a notable transition occurring between the 200-mbar and 500-mbar cases. The greater NO_2 concentrations facilitate faster formation of NO_3, both of which increase the rate of N_2O_5 production.

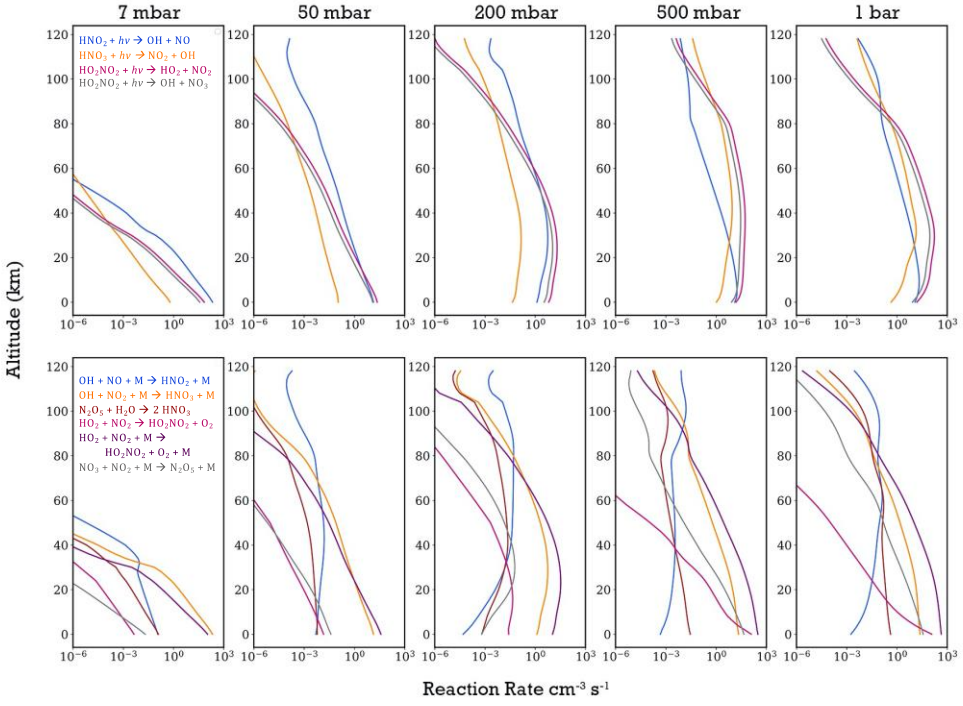

Figure 4. Reaction rates ($cm^{-3}s^{-1}$) for loss by photolysis (upper panel) and production (lower panel) reactions for HNOx species. Different climate scenarios are shown in panels from left to right: 7 mbar, 50 mbar, 200 mbar, 500 mbar, and 1 bar. For clarity within each panel, only the 1x J_{ice} case is shown.

With several assumptions, we can approximate to an order of magnitude the concentration of salts that have accumulated in the Mars soil. We attempt to roughly estimate the duration of each of our four surface pressures by discretizing the rate of atmospheric CO_2 loss described in Hu et al. (2015) and extrapolating back to 4.1 Gya (the start of the Noachian); although we acknowledge these are highly uncertain and that the surface pressure would have likely decreased more smoothly over time: ~300 Myr each in the 1-bar, 500-mbar, 200-mbar,

and 50-mbar climates and the remainder of Mars' history (~3 Gyr) in the 7-mbar climate. From this, we find that most nitrite and nitrate deposition occurs during the 1-bar and 500-mbar climates. Following deposition on ice and settling of the ice to the surface, we assume the soils are mixed throughout a shallow depth due to post-Noachian impactors. We consider ~2m which represents three e-folding depths (Zent 1998). We also assume a soil density of 1 g/cc (Moore and Jakosky, 1989). These assumptions are consistent with those in Smith et al. (2014). We assume the loss rates of nitrate and nitrite following deposition would be negligible. Nitrates in ice cores are thought to be long-lived and have been used as proxies at Earth for studying the occurrence of past SEP events (Dreschhoff & Zeller, 1990; Schrijver et al., 2012). We assume no aqueous systems existed during this part of Mars' history, although short aqueous episodes could have invoked new loss mechanisms including photoreduction, loss to iron, and hydrolysis (Ranjan et al., 2019; Wong et al., 2017). In this scenario, loss to photoreduction would be particularly fast (τ ~1 year; Mack and Bolton, 1999). Under these assumptions, our 1x ice case's deposition fluxes correspond to the following weight percents: ~4 wt% NO from nitrate, ~8 wt% NO from nitrite. This is much greater than the MSL findings (70-1100 ppm; Sutter et al., 2017; Stern et al., 2015), suggesting that nitrate and nitrite were likely altered on Mars' surface and lost over time. This paper only seeks to describe the atmospheric formation of nitrate in the atmosphere and delivery to the surface, so we encourage future works to investigate surface loss processes for surface nitrate in cold climates (such as cosmic rays) or to better constrain the occurrence and duration of short aqueous episodes at Mars through time.

5. Discussion: Interpreting the Formation of MSL-Measured Volatiles

We find that icy climates are able to form and deposit nitric acid fast enough to produce global-average nitrate deposits at least as large as the MSL-measurements, although we acknowledge that the MSL measurements may not be globally representative (e.g., ices and/or NOx could transport to locally collect in some regions).

Our result does not rule out the formation of nitrates in warm and wet climates (e.g., Adams et al., 2021). However, it suggests the nitrates measured by MSL could be formed by two mechanisms at different epochs in time. Future measurements of N-isotopes in the Martian nitrates could help constrain when the nitrates formed. Over Mars' history, the atmospheric isotopic record became enriched in heavy isotopes due to atmospheric loss to space; since nitrate formation originates with atmospheric chemistry under both regimes, nitrates formed during the warm and wet climate would likely be older and thus of lighter isotopic signatures than nitrates formed during the cool, icy climate. Surface loss processes (such as photoreduction in the warm, wet climates) may also influence the abundance of nitrates and nitrites, as well as $^{14}N/^{15}N$.

Our results demonstrate that the deposition of pernitric acid may have been faster than that of nitric acid, in agreement with Smith et al. (2014). Importantly, there appears to be a surface pressure dependence for the total rain out rates of HNOx species *and* the relative rain out rates of pernitric vs nitric acid. The fate of pernitric acid upon deposition may be analogous to its fate in aqueous systems, in which its destruction would result in nitrite salts on the surface (e.g., Regimbal and Mozurkewich, 1997; Slusher et al., 2002). However, Sutter et al. (2017) reports only detections of nitrate at Mars from the SAM instrument, inferred from multiple NO releases from soil samples in the evolved gas analysis (EGA) experiment; they suggest NO peaks at various temperatures may result from NO evolved from different samples including Fe-bearing nitrates, which evolve at relatively lower temperatures, and Mg-, Ca-, Na- and K-bearing

nitrates, which evolve at relatively higher temperatures (e.g., Gordon and Campbell, 1955; Mu and Perlmutter, 1982; Ettarh and Galwey, 1996; Stern et al., 2015).

It may be interesting to question whether the evolved NO could suggest the presence of nitrite. Navarro-González et al. (2018) discovered that both nitrite and nitrate are extremely labile in the presence of iron perchlorates decomposing at temperatures below 270 C; however, in the presence of magnesium and calcium chlorates or perchlorates, $NO2^-$ decomposes below 400 C and nitrate decomposes above 400 C. The EGA results of Sutter et al. (2017) show NO peaks at temperatures below 400 C in the Cumberland, John Klein, and Rocknest samples; NO peaks at temperatures greater than 400 C are in several other samples. We suggest that future work investigate the thermal decomposition of nitrite- and nitrate- bearing species in Mars-like soil samples in order to place better constraints on interpreting the presence or absence of nitrite.

Open Research

KINETICS output files and Python analysis scripts are available at the open-source repository (Adams, 2023).

Acknowledgements

We thank Dr. Glenn Orton and Dr. Steve Vance for helpful comments on the manuscript. Work at the Jet Propulsion Laboratory, California Institute of Technology, is performed under contract with the National Aeronautics and Space Administration (80NM0018D0004).

References

Ackerman, A. S. and Marley, M. S. (2001). Precipitating Condensation Clouds in Substellar Atmospheres. *The Astrophysical Journal*, 556, 2, doi:10.1086/321540

Adams, D., Luo, Y., Wong, M., Dunn, P., Christensen, M., Dong, C., Hu, R., Yung, Y. (2021). Nitrogen Fixation at Early Mars. Astrobiology, 21, 8, 968-980, doi:10.1089/ast.2020.2273

Adams, Danica (2023). "Replication Data for: Nitrogen Fixation at Paleo-Mars in Icy Climates", [Dataset], Harvard Dataverse, https://doi.org/10.7910/DVN/7I7DQF

Adams, D., Scheucher, M., Hu, R., Thomas, T., Scheller, E., Lillis, R., Smith, K., Wordsworth, R., Ehlmann, B., Rauer, H., Yung, Y.. Crustal Hydration Primed Early Mars with Warm and Habitable Conditions, *in review at Nature Geoscience.*

Allen, M., Yung, Y. L., and Waters, J. W. (1981). Vertical transport and photochemistry in the terrestrial mesosphere and lower thermosphere (50-120f km). *Journal of Geophysical Research*, 86, 3617-3627, doi: 10.1029/JA086iA05p03617.

Barnhart, C., Howard, A., Moore, J., Long-term precipitation and late-stage valley network formation: Landform simulations of Parana Basin, Mars. *J. Geophys. Res.* **114**, E1 (2009), doi: 10.1029/2008JE003122

Carr, M. H., and Head, J. W. (2003). Oceans on Mars: An assessment of the observational evidence and possible fate. *J. Geophys. Res. Planets* ***108***, E5, doi: 10.1029/2002JE001963

Claire, M. W., Sheets, J., Cohen, M., Ribas, I., Meadows, V., Catling, D. (2012). The evolution of solar flux from 0.1 nm to 160 um: quantitative estimates for planetary studies. The astrophysical journal, 757, 1, doi:10.1088/0004-637X/757/1/95

S. M. Clifford, T. J. Parker (2001). The evolution of the Martian hydrosphere: Implications for the fate of a primordial ocean and the current state of the northern plains. *Icarus*, ***154***, 40-79, doi: 10.1006/icar.2001.6671

Dreschhoff, G. A. M. and Zeller, E. J. (1990). Evidence of individual solar proton events in antarctic snow. Solar Physics, 127, 2, doi:10.1007/BF00152172

Ettarh, C. and Galwey, A. K. (1996). A kinetic and mechanistic study of the thermal decomposition of calcium nitrate, *Thermochim. Acta*, 288, 203-219, doi: 10.1016/S0040-6031(96)03052-3

Graham, R. A., Winer, A. M., Pitts, J. N. (1978). Pressure and temperature dependence of the unimolecular decomposition of HO_2NO_2. *J. Chem. Phys.,* 68, 4505-4510, doi:10.10163/435554

Gierczak, T., Jimenez, E., Riffault, V., Burkholder, J., Ravishankara, A. (2005). Thermal decomposition of HO2NO2 (peroxynitric acid, PNA): rate coefficient and determination of the enthalpy of formation. *J Phys Chem A,* 109, 4, 586-596, doi:10.1021/jp046632f

Gordon, S. and Campbell, C. (1955). Differential thermal analysis of inorganic compounds: nitrates and perchlorates of alkali and alkaline earth groups and subgroups, Anal. Chem., 27, 1002-1109.

Hoke, M., Hynek, B., Tucker, G. (2011). Formation timescales of large Martian valley networks, *Earth and Planet. Sci. Letters* **312**, 1, doi: 10.1016/j.epsl.2011.09.053

Holm, N. and Neubeck, A. (2009). Reduction of nitrogen compounds in oceanic basement and its implications for HCN formation and abiotic organic synthesis. Geochemical Transactions, 10:9, doi:10.1186/I467-4866-10-9

Hu, R. and Thomas, T. (2022). A nitrogen-rich atmosphere on ancient Mars consistent with isotopic evolution models, *Nature Geoscience* **15**, 2, doi: 10.1038/s41561-021-00886-y

Hunten, D. (1973). The escape of light gases from planetary atmospheres, *J Atmos. Sci.* **30**, 8, doi: 10.1175/1520-0469(1973)030<1481:TEOLGF>2.0.CO;2

Jakosky, B., Brain, D., Chaffin, M., Curry, S., Deighan, J., Grebowsky, J., et al. (2018). Loss of the Martian atmosphere to space: Present-day loss rates determined from MAVEN observations and integrated loss through time, *Icarus* **315**, 146-157, doi: 10.1016/j.icarus.2018.05.030

Kasting, J. F. (1991). CO_2 condensation and the climate of early Mars. Icarus, 94, 1-13, doi: 10.1016/0019-1035(91)90137-I

Kleinböhl, A., Schofield, J. T., Kass, D. M., Abdou, W. A., Backus, C. R., Sen, B., Shirley, J. H, Lawson, W. G., Richardson, M. I., Taylor, F. W., Teanby, N. A., McCleese, D. J., Mars Climate Sounder Limb Profile Retrieval of atmospheric Temperature, Pressure, Dust and Water ice opacity, *J. Geophys. Res.*, *114*, E10006, doi:10.1029/2009JE003358, 2009.

Kleinböhl, A., J. T. Schofield, W. A. Abdou, P. G. J. Irwin, R. J. de Kok, A single-scattering approximation for infrared radiative transfer in limb geometry in the Martian atmosphere, *J. Quant. Spectrosc. Radiat. Transfer, 112,* 1568–1580, doi:10.1016/j.jqsrt.2011.03.006, 2011.

Kleinböhl, A., A. J. Friedson, and J. T. Schofield, Two-dimensional radiative transfer for the retrieval of limb emission measurements in the Martian atmosphere, *J. Quant. Spectrosc. Radiat. Transfer, 187*, 511-522, doi:10.1016/j.jqsrt.2016.07.009, 2017.

Krasnopolsky, V. (1993). Photochemistry of the martian atmosphere (mean conditions). Icarus, 101, 2, 313-332, doi:10.1006/icar.1993.1027

Lui, R., Jia, X., Wang, F., Ren, Y., Wong, X., Zhang, H., Li, G., Wang, X., Tang, M. (2020). Heterogeneous reaction of NO2 with hematite, goethite and magnetite: implications for nitrate formation and iron solubility enhancement. Chemosphere 242, doi:10.1016/j.chemosphere.2019.125273

Mack, J., and Bolton, J.R. (1999) Photochemistry of nitrite and nitrate in aqueous solution: a review. J Photochem Photobiol A Chem 128:1–13, doi: 10.1016/S1010-6030(99)00155-0

Mancinelli, R. L. and McKay, C. P. (1988). The evolution of nitrogen cycling. *Origins of Life and Evolution of the Biosphere,* 18(4), 311-325, doi:10.1007/BF01808213

Mancinelli, R. (1996). The search for nitrogen compounds on the surface of mars. Advances in space research, 18, 12, 241-248, doi:10.1016/0273-1177(96)00113-5

Michelangeli, D., Yung, Y., Allen (1989). El Chichon volcanic aerosols: impact of radiative, thermal, and chemical perturbations. Journal of Geophysical Research: Atmospheres 94, D15, doi:10.1029/JD094iD15p18429

Moore, H. J. and Jakosky B. M. (1989). Viking Landing sites, remote-sensing observations, and physical properties of Martian surface materials. Icarus 81, 1, doi:10.1016/0019-1035(89)90132-2

Moses, J., Fouchet, T., Bezard, B., Gladstone, G., Lellouch, E., Feuchtgruber, H. (2005). Photochemistry and diffusion in Jupiter's stratosphere: constratints from ISO observations and comparisons with other giant planets. Journal of Geophysical Research, 110, E8, doi:10.1029/2005JE002411

Mu, J. and Perlmutter, D. D. (1982). Thermal decomposition metal nitrates and their hydrates. *Thermochim. Acta,* 56, 253-260, doi: 10.1016/0040-6031(82)87033-0

Nair, H., Allen, M., Anbar, A., Yung, Y., Clancy, R. T. (1994). A photochemical model of the martian atmosphere. Icarus, 111, 1, 124-150, doi:10.1006/icar.1994.1137

Navarro-González, R., Coll, P., Sutter, B., Stern, J. C., McKay, C. P., Martin-Torres, F. J., Zorzano-Mier, M.-P., Archer, P. D., et al. (2018). Detection of nitrites by the Sample Analysis at Mars (SAM) Instrument. Implications for the Oxidation State of the Atmosphere. 49th Lunar and Planetary Science Conference 19-23 March, 2018.

Nordheim, T. A., L. R. Dartnell, L. Desorgher, A. J. Coates, and G. H. Jones, Ionization of the Venusian atmosphere from solar and galactic cosmic rays, *Icarus*, 245, 80-86, doi: 10.1016/j.icarus.2014.09.032, 2015.

Olsen, A. and Rimstidt, J. D. Using a mineral lifetime diagram to evaluate the persistence of olivine on Mars. *American Mineralogist,* 92, 4 (2007), doi: 10.2138/am.2007.2462

Ranjan, S., Todd, Z., Rimmer, P., Sasselov, D., and Babbin, A. (2019). Nitrogen oxide concentrations in natural waters on early Earth. *Geochemistry, Geophysics, Geosystems, 20,* 2021-2039, doi:10.1029/2018GC008082

Regimbal, J.-M. and Mozurkewich, M. (1997). Peroxynitric acid decay mechanisms and kinetics at low pH. The Journal of Physical Chemistry A, 101, 47, doi:10.1021/jp971908n

Schrijver, C. J., Beer, J., Baltensperger, U., Cliver, E., Gudel, M., Hudson, H., McCracken, K., Osten, R., et al. (2012). Journal of Geophysical Research: Space Physics, 117, A8, doi:10.1029/2012JA017706

Slusher, D. L., Huey, L. G., Tanner, D. J., Chen, G., Davis, D., D., Buhr, M., Nowack, J. B., et al. (2002). Measurements of pernitric acid at the south pole during ISCAT 2000. Geophysical Research Letters 29, 21, doi:10.1029/2002GL015703

Smith, M. L., Claire, M. W., Catling, D., Zahnle, K. (2014). The formation of sulfate, nitrate, and perchlorate salts in the martian atmosphere. Icarus, 231, 51-64, doi:10.1016/j.icarus.2013.11.031

Stern, J. C., Sutter, B., Freissinet, C., Navarro-Gonzalez, R., McKay, C. P., Archer, P. D. Jr., Buch, A., Brunner, A. E., Coll, P., Eigenbrode, J. L., Fairen, A. G., Franz, H. B., Glavin, D. P., Kashyap, S., McAdam, A. C., Ming, D. W., Steele, A., Szopa, C., Wray, J., Martin-Torres, F., Zorzano, M.-P., Conrad, P., Mahaffy, P., and the MSL Science Team (2015). Evidence for indigenous nitrogen in sedimentary and aeolian deposits from the Curiosity rover investigations at Gale crater, Mars. *Proceedings of the National Academy of Sciences of the United States of America,* 112(14), 4245-4250, doi:10.1073/pnas.1420932112

Sutter, B., McAdams, A. C., Mahaffy, P., Ming, D., Edgett, K., Rampe, E., Eigenbrode, J. L., et. al. (2017). Evolved gas analyses of sedimentary rocks and eolian sediment in Gale Crater, Mars: Results of the Curiosity Rover's sample analysis at Mars instrument from Yellowknife Bay to the Namib Dune. *Journal of Geophysical Research: Planets*, 122, 2574-2609, doi:10.1002/2016JE005225

Trainer, M., Wong, M. H., McConnochie, T. H., Franz, H., Atreya, S., Conrad, P., Lefevre, F., Mahaffy, P., et al. (2019). Seasonal variations in atmospheric composition as measured in Gale Crater, Mars. Journal of Geophysical Research: Planets, 124, 11, doi:10.1029/2019JE006175

Wong, M., Yung, Y., Gladstone, R. (2015). Pluto's implications for a snowball Titan. Icarus, 246, 192-196, doi:10.1016/j.icarus.2014.05.019

Wong, M., Charnay, B., Gao, P., Yung, Y., Russell, M. (2017). Nitrogen Oxides in Early Earth's Atmosphere as Electron Acceptors for Life's Emergence. Astrobiology, 17, 10, 975-983, doi:10.1089/ast.2016.1473

Wordsworth, R. (2016). The climate of Early Mars. Annual Review of Earth and Planetary Sciences, 44, 381-408, doi:10.1146/annurev-earth-060115-012355

Wordsworth, R., Kalugina, Y., Lokshtanov, S., Vigasin, A., Ehlmann, B., Head, J., Sanders, C., Wang, H. (2017). Transient reducing greenhouse warming on early Mars. *Geophysical Research Letters*, 44(2), 665-671, doi:10.1002/2016GL071766

Yung, Y., Strobel, D., Kong, T. Y., McElroy, M. B. (1977). Photochemistry of nitrogen in the martian atmosphere. Icarus, 30, 1, 26-41, doi:10.1016/0019-1035(77)90118-X

Yung, Y. and Demore, W. B. (1982). Photochemistry of the stratosphere of Venus: implications for atmospheric evolution. Icarus, 51, 2, doi:10.1016/0019-1035(82)90080-X

Y. L. Yung & W. B. DeMore, *Photochemistry of Planetary Atmospheres* (Oxford University Press, Oxford, UK, 1998).

Figure 1.

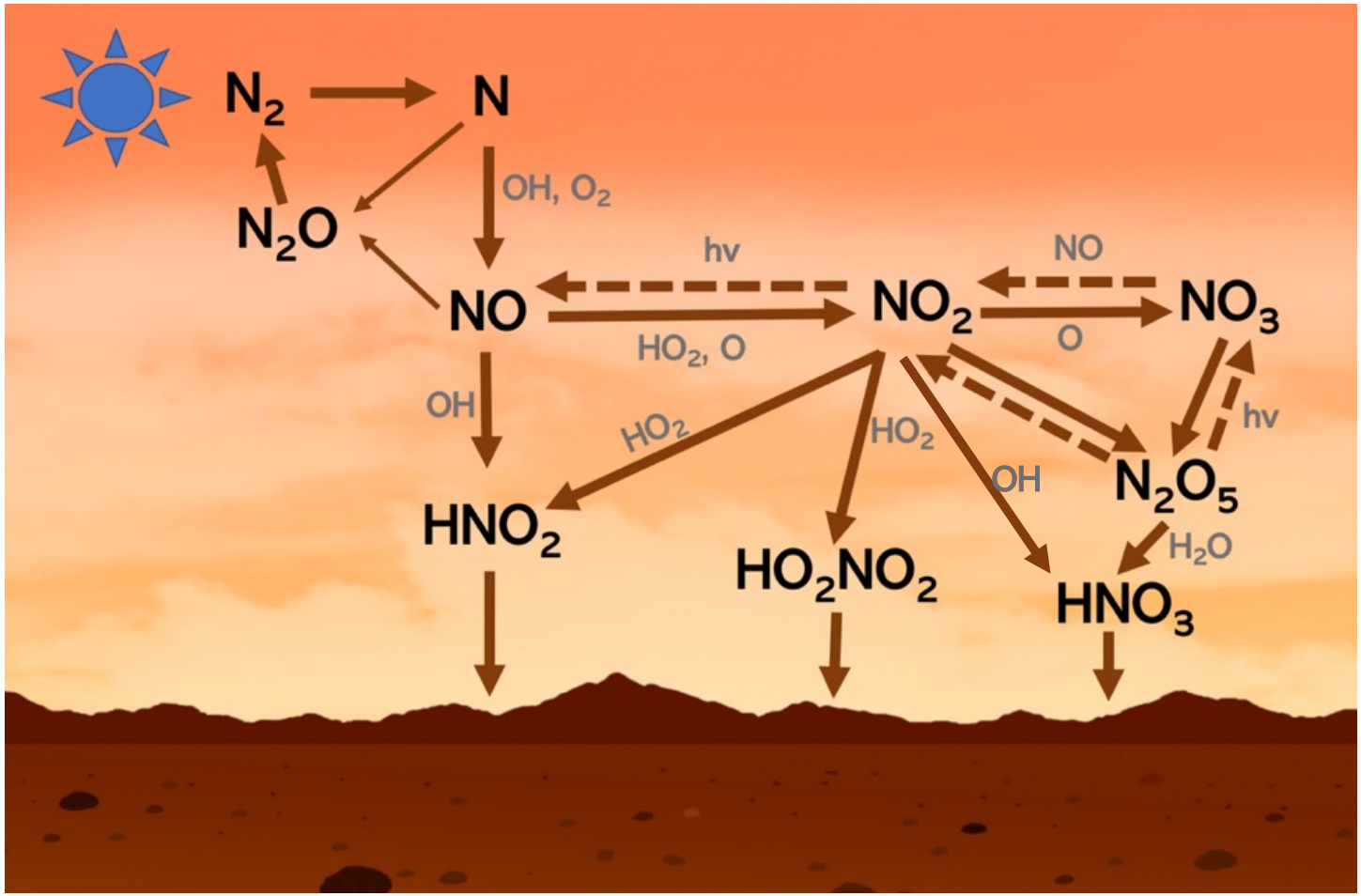
N_2
N
N_2O
OH, O_2
hv
NO
NO
NO_2
NO_3
HO_2, O
O
OH
HO_2
HO_2
hv
OH
N_2O_5
HNO_2
HO_2NO_2
H_2O
HNO_3

Figure 2.

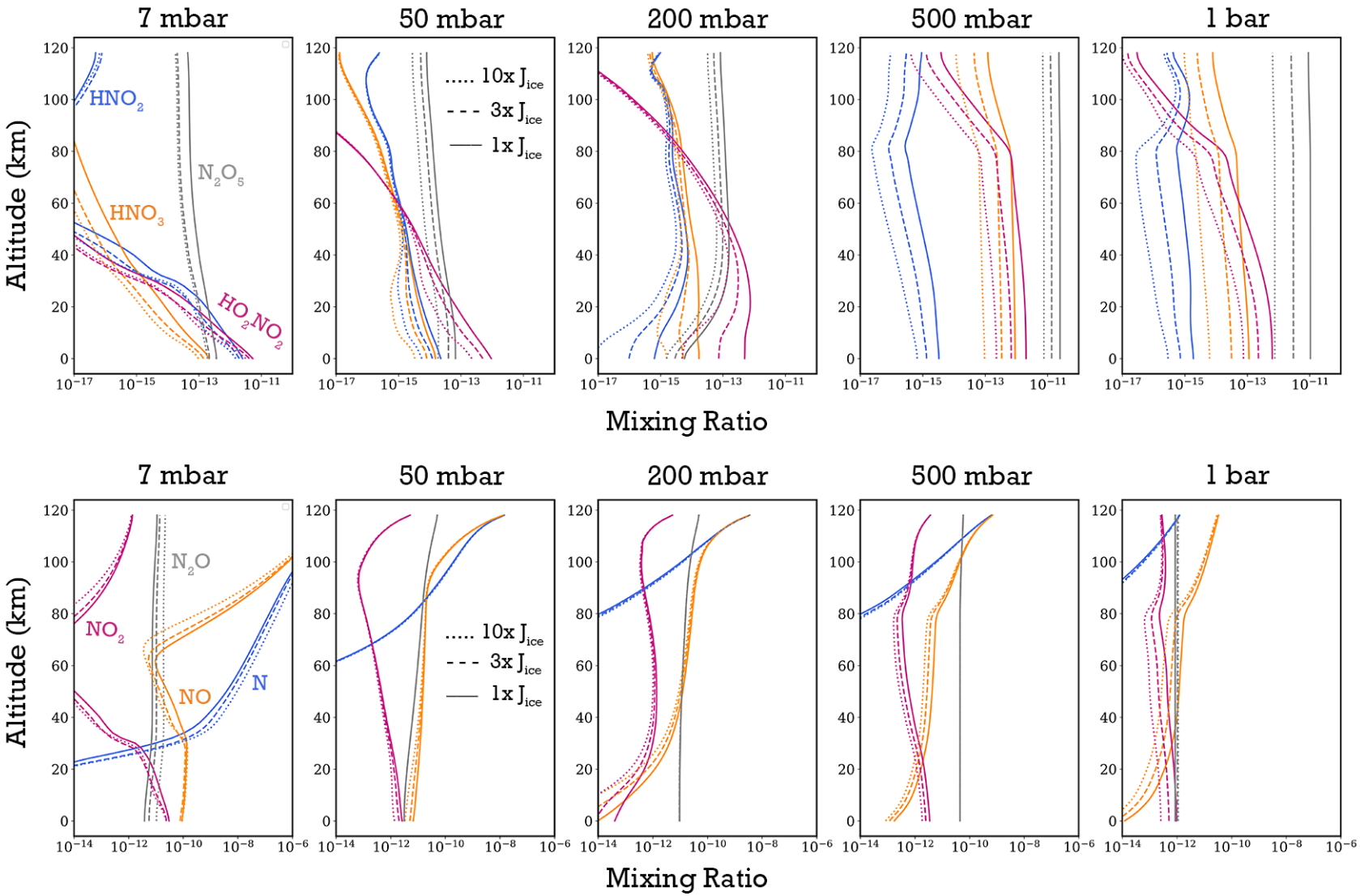
7 mbar
50 mbar
200 mbar
500 mbar
1 bar
Altitude (km)
HNO2
HNO3
N2O5
HO2NO2
..... 10x Jice
--- 3x Jice
—— 1x Jice
Mixing Ratio
N2O
NO2
NO
N

Figure 3.

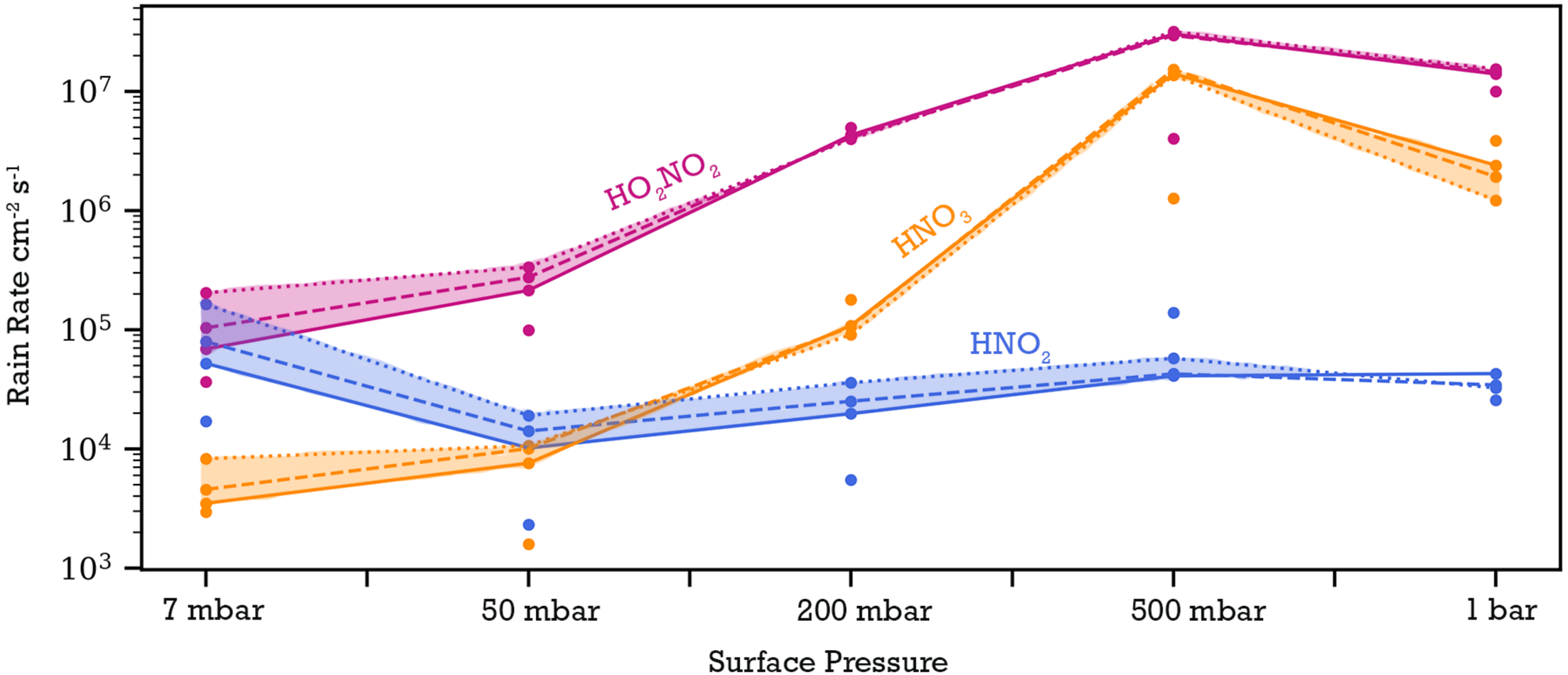
10^7
10^6
10^5
10^4
10^3
Rain Rate cm^{-2} s^{-1}
HO_2NO_2
HNO_3
HNO_2
7 mbar
50 mbar
200 mbar
500 mbar
1 bar
Surface Pressure

Figure 4.

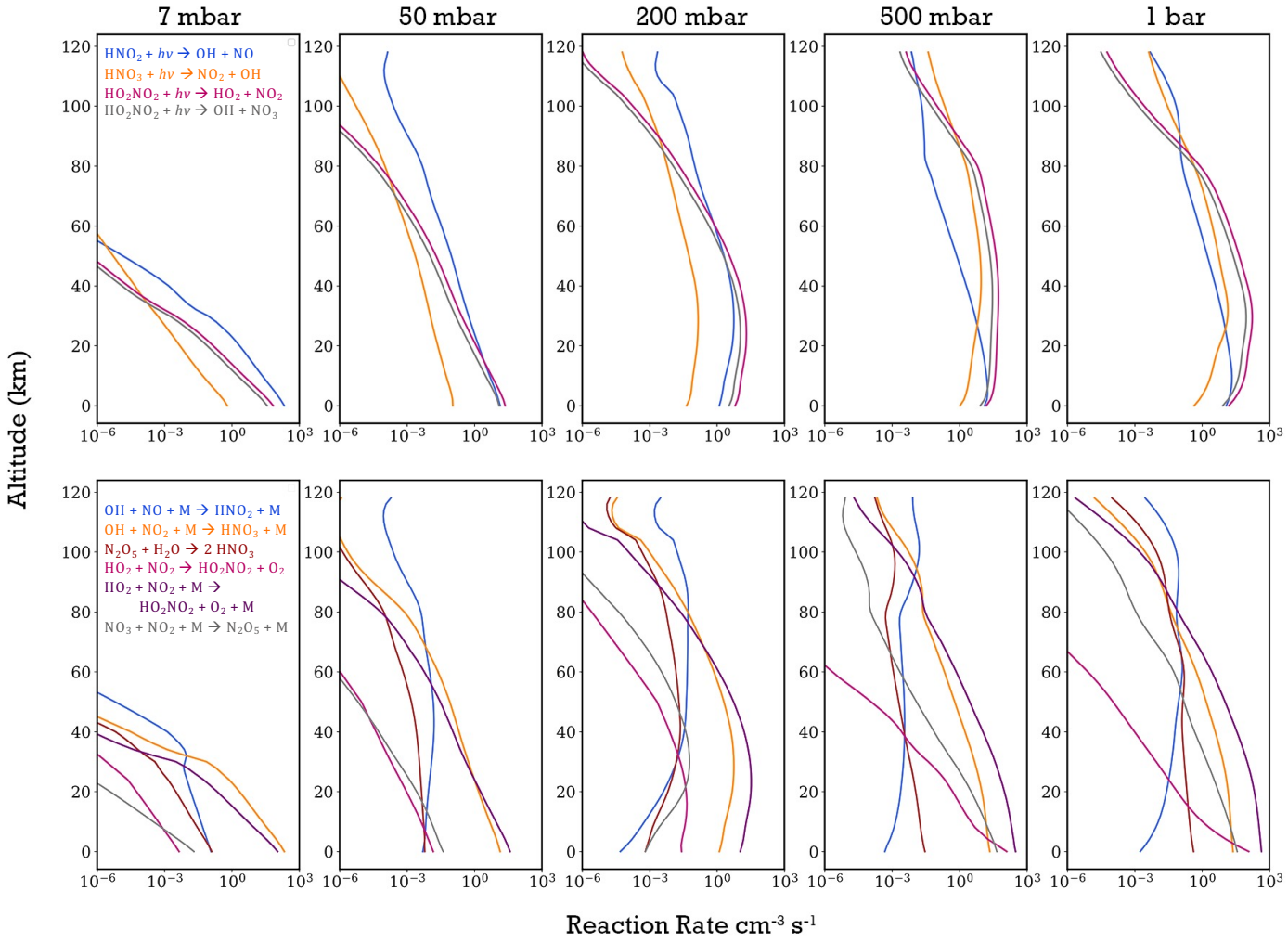
7 mbar
50 mbar
200 mbar
500 mbar
1 bar
Altitude (km)
Reaction Rate cm-3 s-1
HNO2 + hν → OH + NO
HNO3 + hν → NO2 + OH
HO2NO2 + hν → HO2 + NO2
HO2NO2 + hν → OH + NO3
OH + NO + M → HNO2 + M
OH + NO2 + M → HNO3 + M
N2O5 + H2O → 2 HNO3
HO2 + NO2 → HO2NO2 + O2
HO2 + NO2 + M → HO2NO2 + O2 + M
NO3 + NO2 + M → N2O5 + M